J. Plasma Physics (2009), *vol.* 75, *part* 2, *pp.* 203–215. © 2008 Cambridge University Press
doi:10.1017/S0022377808007356 Printed in the United Kingdom

Alfvén eigenmodes in magnetic X-point configurations with strong longitudinal fields

N. BEN AYED[1], K. G. McCLEMENTS[2] and A. THYAGARAJA[2]

[1]Department of Physics, University of York, Heslington, York YO10 5DD, UK (nizar.benayed@ukaea.org.uk)

[2]EURATOM/UKAEA Fusion Association, Culham Science Centre, Abingdon, Oxfordshire OX14 3DB, UK

(Received 18 March 2008, accepted 2 April 2008, first published online 18 July 2008)

Abstract. A perturbative three-dimensional analysis is presented of Alfvén waves in a magnetic X-point configuration with a strong longitudinal guide field. The waves are assumed to propagate in the direction of the X-line, and both the plasma beta and equilibrium plasma current are taken to be zero. This provides a simple model of Alfvén wave propagation in the divertor region of tokamak plasmas. It is shown that the presence of the X-point places constraints on the structure of the leading-order (shear Alfvén) eigenfunctions. These eigenfunctions, and fast wave corrections to them, are determined explicitly for two cases. In the first of these the stream function for the shear Alfvén flow is azimuthally symmetric in the X-point plane and singular at the X-line; in the second case the stream function is largely confined to two quadrants in the X-point plane and is non-singular. For the latter scenario it is shown that coupling of the shear and fast waves is strongly localized to the vicinity of the separatrix.

1. Introduction

The complex magnetohydrodynamic (MHD) properties of magnetic X-points have attracted much attention, due to the fact that configurations with this type of topology are common to many laboratory and natural plasma environments and play a key role in processes such as magnetic reconnection and mode conversion of MHD waves. The fast magnetoacoustic wave is of particular importance in this context since, unlike the shear Alfvén wave, it can carry free magnetic energy into the X-point itself where it can be efficiently transformed into heat, mass flows or energetic particles (Craig and Watson 1992; McClements et al. 2004; McLaughlin and Hood 2004; McKay et al. 2007). The shear wave is also of interest, however, since, except for the special case in which there is no longitudinal field $B_\parallel$ and no variations in that direction, the presence of an X-point causes the shear and fast waves to be coupled (Bulanov and Syrovatskii 1980). Bulanov et al. (1992) studied this coupling analytically for the case of an X-point with zero equilibrium current but finite $B_\parallel$, variations in the longitudinal direction being neglected. They showed that the coupling is associated with the formation of singular structures in

https://doi.org/10.1017/S0022377808007356 Published online by Cambridge University Press

the current density near the X-point separatrix. McClements et al. (2006) solved the initial value problem of a fast wave being driven up by a shear wave for the case in which $B_\parallel$ is smaller than $B_\perp$, the field in the X-point plane, taking into account resistivity and electron inertial effects; again, variations in the longitudinal direction were neglected.

In this paper we extend the analyses of previous authors to three dimensions by allowing for the possibility of wave propagation in the longitudinal (guide-field) direction. This extension is motivated in part by the fact that a current-free X-point with a longitudinal guide field provides a simple model of the divertor region of tokamak plasmas (Farina et al. 1993): the magnetic field at the divertor X-point separatrix is purely toroidal, and the plasma current density in its vicinity is close to zero. However, MHD perturbations to tokamak plasmas are generally not axisymmetric and thus, in the cylinder approximation that we are adopting, it is appropriate to allow longitudinal propagation. Myra et al. (2000) investigated the effect of a tokamak divertor X-point on MHD and two-fluid instabilities, but restricted their MHD analysis to the shear Alfvén branch. We include fast wave physics in our model, assume the tokamak ordering $B_\parallel \gg B_\perp$ and take the limit of zero plasma pressure, which is appropriate for the relatively cool divertor region of tokamak plasmas. It is possible that an improved understanding of the coupling of ideal MHD modes close to the boundary of divertor tokamaks can shed light on edge-localized phenomena observed in such devices, such as the production of filament structures (Kirk et al. 2006). Our analysis may also have applications to internal magnetic islands in tokamaks (Donné et al. 2005) and to X-point configurations in space plasmas, for example in the solar corona (McClymont and Craig 1996).

After defining our equilibrium configuration in Sec. 2, we present in Sec. 3 a perturbative analysis of the cold plasma ideal MHD equations for that equilibrium, using as the perturbation parameter $\lambda \equiv B_\perp/B_\parallel$. We obtain in the process a general solution for the eigenmode structure of Alfvén waves propagating transverse to the plane of a current-free X-point. Our results are summarized and discussed in Sec. 4.

2. Equilibrium field

To determine the mode structure of shear Alfvén waves around a magnetic X-point we begin by considering a uniform equilibrium field

$$\mathbf{B}_E = B_\parallel \hat{\mathbf{z}}, \tag{1}$$

where $B_\parallel$ is a constant and $\hat{\mathbf{z}}$ is the unit vector in the z-direction. Transverse incompressible (shear Alfvén) waves propagating along $\hat{\mathbf{z}}$ are described by functions $f(x, y, z \pm c_A t)$ where $c_A^2 = B_\parallel^2/\mu_0\rho_0$, with μ_0 being the permeability of free space and ρ_0 the equilibrium plasma density, which is assumed throughout this paper to be uniform. Although the actual plasma density in the vicinity of a tokamak divertor X-point is far from uniform, the density gradients are relatively unimportant for Alfvén modes, whose frequencies greatly exceed those of drift waves under typical tokamak conditions. It should be noted that for the equilibrium defined by (1) the dependence of shear Alfvén wave solutions f on x and y is completely arbitrary except for the requirement that the flow perturbation $\tilde{\mathbf{V}}^{(0)}$ be divergence free, i.e. $\partial\tilde{V}_x^{(0)}/\partial x + \partial\tilde{V}_y^{(0)}/\partial x = 0$.

https://doi.org/10.1017/S0022377808007356 Published online by Cambridge University Press

We now consider the effect of adding a current-free X-point field to this equilibrium:

$$\mathbf{B}_E = B_\parallel \hat{\mathbf{z}} + \frac{B_\perp}{r_0}(y\hat{\mathbf{x}} + x\hat{\mathbf{y}}), \tag{2}$$

where $B_\perp$, r_0 are constants and $\hat{\mathbf{x}}$, $\hat{\mathbf{y}}$ denote unit vectors in the x- and y-directions. The (x, y) components of the equilibrium field can be obtained from the flux function

$$\psi_E = \frac{B_\perp}{2r_0}(y^2 - x^2). \tag{3}$$

We take the limit $B_\perp/B_\parallel \equiv \lambda \ll 1$ and write the total equilibrium field in the non-dimensional form

$$\mathbf{b}_E = \mathbf{b}^{(0)} + \lambda \mathbf{b}^{(1)}, \tag{4}$$

where $\mathbf{b}_E = \mathbf{B}_E/B_\parallel$, $\mathbf{b}^{(0)} = \hat{\mathbf{z}}$ and $\mathbf{b}^{(1)} = (y\hat{\mathbf{x}} + x\hat{\mathbf{y}})/r_0$. Throughout this paper superscripts (0) and (1) denote the zeroth- and first-order quantities, respectively.

3. Perturbative analysis

In the limit of zero plasma pressure and equilibrium flow the linearized ideal MHD momentum and induction equations are

$$\frac{\partial \tilde{\mathbf{V}}}{\partial t} = \frac{1}{\rho_0 \mu_0}(\nabla \times \tilde{\mathbf{B}}) \times \mathbf{B}_E, \tag{5}$$

$$\frac{\partial \tilde{\mathbf{B}}}{\partial t} = \nabla \times (\tilde{\mathbf{V}} \times \mathbf{B}_E), \tag{6}$$

where $\tilde{\mathbf{B}}$ and $\tilde{\mathbf{V}}$ are the perturbations to the magnetic field and fluid velocity. Before proceeding further with these equations, we normalize the space coordinates x, y and z to r_0, $\tilde{\mathbf{B}}$ to $B_\parallel$, $\tilde{\mathbf{V}}$ to c_A and t to r_0/c_A. We also express the velocity and field perturbations as power series in λ:

$$\tilde{\mathbf{V}} = \tilde{\mathbf{V}}^{(0)} + \lambda \tilde{\mathbf{V}}^{(1)} + \lambda^2 \tilde{\mathbf{V}}^{(2)} + \cdots, \tag{7}$$

$$\tilde{\mathbf{B}} = \tilde{\mathbf{B}}^{(0)} + \lambda \tilde{\mathbf{B}}^{(1)} + \lambda^2 \tilde{\mathbf{B}}^{(2)} + \cdots. \tag{8}$$

We now proceed to substitute (7) and (8) into the dimensionless forms of (5) and (6), equating terms in powers of λ.

3.1. Zeroth-order equations

Using (4) into (5) and (6), and equating terms that are independent of λ, we obtain

$$\frac{\partial \tilde{\mathbf{V}}^{(0)}}{\partial t} = \left(\nabla \times \tilde{\mathbf{B}}^{(0)}\right) \times \mathbf{b}^{(0)}, \tag{9}$$

$$\frac{\partial \tilde{\mathbf{B}}^{(0)}}{\partial t} = \nabla \times \left(\tilde{\mathbf{V}}^{(0)} \times \mathbf{b}^{(0)}\right). \tag{10}$$

It is apparent from the z-component of (9) that $\tilde{V}_z^{(0)}$ is a constant of the motion: we set $\tilde{V}_z^{(0)} = 0$ for convenience. The z-component of (10) is

$$\frac{\partial \tilde{B}_z^{(0)}}{\partial t} = -\left(\frac{\partial \tilde{V}_x^{(0)}}{\partial x} + \frac{\partial \tilde{V}_y^{(0)}}{\partial y}\right). \tag{11}$$

https://doi.org/10.1017/S0022377808007356 Published online by Cambridge University Press

Since, in zeroth order, we are seeking incompressible (shear Alfvén) wave solutions, it is appropriate to assume that $\nabla\cdot\tilde{\mathbf{V}}^{(0)}=0$: since $\tilde{V}_z^{(0)}=0$ it follows from (11) that $\tilde{B}_z^{(0)}$ is a constant of the motion, which we also set equal to zero. The remaining components of (9) and (10),

$$\frac{\partial\tilde{V}_x^{(0)}}{\partial t}=\frac{\partial\tilde{B}_x^{(0)}}{\partial z}, \tag{12}$$

$$\frac{\partial\tilde{V}_y^{(0)}}{\partial t}=\frac{\partial\tilde{B}_y^{(0)}}{\partial z}, \tag{13}$$

$$\frac{\partial\tilde{B}_x^{(0)}}{\partial t}=\frac{\partial\tilde{V}_x^{(0)}}{\partial z}, \tag{14}$$

$$\frac{\partial\tilde{B}_y^{(0)}}{\partial t}=\frac{\partial\tilde{V}_y^{(0)}}{\partial z}, \tag{15}$$

then describe wave propagation at unit velocity in the longitudinal direction.

3.2. *First-order equations*

Equating coefficients of λ in the momentum and induction equations, we obtain

$$\frac{\partial\tilde{\mathbf{V}}^{(1)}}{\partial t}=\left(\nabla\times\tilde{\mathbf{B}}^{(0)}\right)\times\mathbf{b}^{(1)}+\left(\nabla\times\tilde{\mathbf{B}}^{(1)}\right)\times\mathbf{b}^{(0)},$$

$$\frac{\partial\tilde{\mathbf{B}}^{(1)}}{\partial t}=\nabla\times\left(\tilde{\mathbf{V}}^{(0)}\times\mathbf{b}^{(1)}\right)+\nabla\times\left(\tilde{\mathbf{V}}^{(1)}\times\mathbf{b}^{(0)}\right).$$

With $\tilde{V}_z^{(0)}=\tilde{B}_z^{(0)}=0$, the components of these equations are

$$\frac{\partial\tilde{V}_x^{(1)}}{\partial t}-\frac{\partial\tilde{B}_x^{(1)}}{\partial z}+\frac{\partial\tilde{B}_z^{(1)}}{\partial x}=x\left(\frac{\partial\tilde{B}_x^{(0)}}{\partial y}-\frac{\partial\tilde{B}_y^{(0)}}{\partial x}\right), \tag{16}$$

$$\frac{\partial\tilde{V}_y^{(1)}}{\partial t}-\frac{\partial\tilde{B}_y^{(1)}}{\partial z}+\frac{\partial\tilde{B}_z^{(1)}}{\partial y}=y\left(\frac{\partial\tilde{B}_y^{(0)}}{\partial x}-\frac{\partial\tilde{B}_x^{(0)}}{\partial y}\right), \tag{17}$$

$$\frac{\partial\tilde{V}_z^{(1)}}{\partial t}=-x\frac{\partial\tilde{B}_y^{(0)}}{\partial z}-y\frac{\partial\tilde{B}_x^{(0)}}{\partial z}, \tag{18}$$

$$\frac{\partial\tilde{B}_x^{(1)}}{\partial t}-\frac{\partial\tilde{V}_x^{(1)}}{\partial z}=x\frac{\partial\tilde{V}_x^{(0)}}{\partial y}-\tilde{V}_y^{(0)}-y\frac{\partial\tilde{V}_y^{(0)}}{\partial y}, \tag{19}$$

$$\frac{\partial\tilde{B}_y^{(1)}}{\partial t}-\frac{\partial\tilde{V}_y^{(1)}}{\partial z}=y\frac{\partial\tilde{V}_y^{(0)}}{\partial x}-\tilde{V}_x^{(0)}-x\frac{\partial\tilde{V}_x^{(0)}}{\partial x}, \tag{20}$$

$$\frac{\partial\tilde{B}_z^{(1)}}{\partial t}+\frac{\partial\tilde{V}_x^{(1)}}{\partial x}+\frac{\partial\tilde{V}_y^{(1)}}{\partial y}=0. \tag{21}$$

The zeroth-order equations for $\tilde{\mathbf{V}}$ and $\tilde{\mathbf{B}}$ are recovered when the forcing terms on the right-hand sides of (16)–(21) are neglected. Differentiating (16) and (17) with respect to time, using (14) and (15) to eliminate $\tilde{B}_x^{(0)}$ and $\tilde{B}_y^{(0)}$, we obtain a pair of

https://doi.org/10.1017/S0022377808007356 Published online by Cambridge University Press

coupled second-order equations for $\tilde{V}_x^{(1)}$ and $\tilde{V}_y^{(1)}$:

$$\frac{\partial^2 \tilde{V}_x^{(1)}}{\partial t^2} - \frac{\partial^2 \tilde{V}_x^{(1)}}{\partial z^2} - \frac{\partial^2 \tilde{V}_x^{(1)}}{\partial x^2} - \frac{\partial^2 \tilde{V}_y^{(1)}}{\partial x \partial y}$$
$$= \frac{\partial}{\partial z}\left(2x\frac{\partial \tilde{V}_x^{(0)}}{\partial y} - x\frac{\partial \tilde{V}_y^{(0)}}{\partial x} - \tilde{V}_y^{(0)} - y\frac{\partial \tilde{V}_y^{(0)}}{\partial y}\right), \tag{22}$$

$$\frac{\partial^2 \tilde{V}_y^{(1)}}{\partial t^2} - \frac{\partial^2 \tilde{V}_y^{(1)}}{\partial z^2} - \frac{\partial^2 \tilde{V}_x^{(1)}}{\partial x \partial y} - \frac{\partial^2 \tilde{V}_y^{(1)}}{\partial y^2}$$
$$= \frac{\partial}{\partial z}\left(2y\frac{\partial \tilde{V}_y^{(0)}}{\partial x} - y\frac{\partial \tilde{V}_x^{(0)}}{\partial y} - \tilde{V}_x^{(0)} - x\frac{\partial \tilde{V}_x^{(0)}}{\partial x}\right). \tag{23}$$

It is appropriate at this stage to introduce two new variables, $\chi^{(1)}$ and $\Lambda^{(1)}$, defined respectively as the divergence of $\tilde{\mathbf{V}}^{(1)}$ in the X-point plane and the longitudinal component of the first-order vorticity:

$$\chi^{(1)} \equiv \frac{\partial \tilde{V}_x^{(1)}}{\partial x} + \frac{\partial \tilde{V}_y^{(1)}}{\partial y}, \tag{24}$$

$$\Lambda^{(1)} \equiv \frac{\partial \tilde{V}_x^{(1)}}{\partial y} - \frac{\partial \tilde{V}_y^{(1)}}{\partial x}. \tag{25}$$

Differentiating (22) with respect to x, (23) with respect to y and summing, we obtain

$$\frac{\partial^2 \chi^{(1)}}{\partial t^2} - \nabla^2 \chi^{(1)} = \frac{\partial}{\partial z}\left(-x\frac{\partial^2 \tilde{V}_y^{(0)}}{\partial x^2} + x\frac{\partial^2 \tilde{V}_x^{(0)}}{\partial x \partial y} - y\frac{\partial^2 \tilde{V}_x^{(0)}}{\partial y^2} + y\frac{\partial^2 \tilde{V}_y^{(0)}}{\partial x \partial y}\right). \tag{26}$$

Similarly, differentiating (23) with respect to x, (22) with respect to y and subtracting, we obtain

$$\frac{\partial^2 \Lambda^{(1)}}{\partial t^2} - \frac{\partial^2 \Lambda^{(1)}}{\partial z^2} = \frac{\partial}{\partial z}\left(-x\frac{\partial^2 \tilde{V}_y^{(0)}}{\partial y \partial x} + 2x\frac{\partial^2 \tilde{V}_x^{(0)}}{\partial y^2} - 2\frac{\partial \tilde{V}_y^{(0)}}{\partial y} - y\frac{\partial^2 \tilde{V}_y^{(0)}}{\partial y^2}\right)$$
$$+ \frac{\partial}{\partial z}\left(-2y\frac{\partial^2 \tilde{V}_y^{(0)}}{\partial x^2} + y\frac{\partial^2 \tilde{V}_x^{(0)}}{\partial y \partial x} + 2\frac{\partial \tilde{V}_x^{(0)}}{\partial x} + x\frac{\partial^2 \tilde{V}_x^{(0)}}{\partial x^2}\right). \tag{27}$$

We now assume that all perturbed quantities have a variation in z and t of the form $\exp[i(k_z z - \omega t)]$. Recalling that the zeroth-order flow $\tilde{\mathbf{V}}^{(0)}$ is divergence-free, we also introduce a stream function $A(x, y)$ for this flow:

$$\tilde{V}_x^{(0)} = \frac{\partial A}{\partial y}\exp[i(k_z z - \omega t)], \tag{28}$$

$$\tilde{V}_y^{(0)} = -\frac{\partial A}{\partial x}\exp[i(k_z z - \omega t)]. \tag{29}$$

It is straightforward to verify that (27) then takes the form

$$-(\omega^2 - k_z^2)\Lambda^{(1)} = 2ik_z\left[\left(x\frac{\partial}{\partial y} + y\frac{\partial}{\partial x}\right)\nabla_\perp^2 A + 2\frac{\partial^2 A}{\partial x \partial y}\right], \tag{30}$$

https://doi.org/10.1017/S0022377808007356 Published online by Cambridge University Press

where

$$\nabla_\perp^2 \equiv \frac{\partial^2}{\partial x^2} + \frac{\partial^2}{\partial y^2}.$$

Fourier analysis in z and t of the leading-order equations (12)–(15) leads to the shear Alfvén wave dispersion relation, which in our dimensionless units takes the form $\omega = k_z$. Considering specifically solutions of the above equations that satisfy this dispersion relation, we infer from (30) that for $k_z \neq 0$ the stream function A must satisfy the equation

$$\left(x\frac{\partial}{\partial y} + y\frac{\partial}{\partial x}\right)\nabla_\perp^2 A + 2\frac{\partial^2 A}{\partial x \partial y} = 0. \tag{31}$$

As discussed at the beginning of this section, a shear wave propagating in the z-direction in a strictly uniform plasma may be ascribed a completely arbitrary structure in the (x, y)-plane. The above compatibility relation indicates that this arbitrariness is removed by introducing an X-point to the field topology.

In a similar fashion, Fourier analysis in z and t of (26) leads to the equation

$$\left(\omega^2 - k_z^2\right)\chi^{(1)} + \nabla_\perp^2 \chi^{(1)} = ik_z\left(y\frac{\partial}{\partial y} - x\frac{\partial}{\partial x}\right)\nabla_\perp^2 A. \tag{32}$$

Applying again the dispersion relation $\omega = k_z$, this reduces to

$$\nabla_\perp^2 \chi^{(1)} = ik_z\left(y\frac{\partial}{\partial y} - x\frac{\partial}{\partial x}\right)\nabla_\perp^2 A. \tag{33}$$

We note also that Fourier analysis in z and t of (16)–(21) yields

$$-i\omega\tilde{V}_x^{(1)} - ik_z\tilde{B}_x^{(1)} + \frac{\partial \tilde{B}_z^{(1)}}{\partial x} = -x\left(\frac{\partial^2 A}{\partial y^2} + \frac{\partial^2 A}{\partial x^2}\right), \tag{34}$$

$$-i\omega\tilde{V}_y^{(1)} - ik_z\tilde{B}_y^{(1)} + \frac{\partial \tilde{B}_z^{(1)}}{\partial y} = y\left(\frac{\partial^2 A}{\partial x^2} + \frac{\partial^2 A}{\partial y^2}\right), \tag{35}$$

$$-i\omega\tilde{V}_z^{(1)} = ik_z\left(-x\frac{\partial A}{\partial x} + y\frac{\partial A}{\partial y}\right), \tag{36}$$

$$-i\omega\tilde{B}_x^{(1)} - ik_z\tilde{V}_x^{(1)} = x\frac{\partial^2 A}{\partial y^2} + \frac{\partial A}{\partial x} + y\frac{\partial^2 A}{\partial x \partial y}, \tag{37}$$

$$-i\omega\tilde{B}_y^{(1)} - ik_z\tilde{V}_y^{(1)} = -y\frac{\partial^2 A}{\partial x^2} - \frac{\partial A}{\partial y} - x\frac{\partial^2 A}{\partial x \partial y}, \tag{38}$$

$$-i\omega\tilde{B}_z^{(1)} + \chi^{(1)} = 0. \tag{39}$$

3.3. Solutions

To find solutions of the above equations it is convenient to Fourier transform them in x and y: specifically, we define the Fourier transform $\hat{f}(k_x, k_y)$ of a general function $f(x, y)$ by the expression

$$\hat{f}(k_x, k_y) = \iint f(x, y)\exp[-i(k_x x + k_y y)]\frac{dx}{\sqrt{2\pi}}\frac{dy}{\sqrt{2\pi}}.$$

https://doi.org/10.1017/S0022377808007356 Published online by Cambridge University Press

It is straightforward to establish that in (k_x, k_y)-space (31) takes the form

$$\left(k_y \frac{\partial}{\partial k_x} + k_x \frac{\partial}{\partial k_y}\right) \hat{A}(k_x, k_y) = -2 \frac{k_x k_y}{k_x^2 + k_y^2} \hat{A}(k_x, k_y), \tag{40}$$

while the compressibility equation (33) is transformed to

$$\left(k_x^2 + k_y^2\right) \hat{\chi}^{(1)} = i\omega \left(k_x \frac{\partial}{\partial k_x} - k_y \frac{\partial}{\partial k_y}\right) \left(k_x^2 + k_y^2\right) \hat{A}. \tag{41}$$

Note that $\hat{\chi}^{(1)}$ and $\hat{\Lambda}^{(1)}$ are related to the Fourier transformed (x, y) velocity components by

$$\hat{\chi}^{(1)} = ik_x \hat{V_x}^{(1)} + ik_y \hat{V_y}^{(1)},$$

$$\hat{\Lambda}^{(1)} = ik_y \hat{V_x}^{(1)} - ik_x \hat{V_y}^{(1)},$$

and hence

$$\hat{V_x}^{(1)} = -i \frac{k_x}{k_x^2 + k_y^2} \hat{\chi}^{(1)} - i \frac{k_y}{k_x^2 + k_y^2} \hat{\Lambda}^{(1)},$$

$$\hat{V_y}^{(1)} = -i \frac{k_y}{k_x^2 + k_y^2} \hat{\chi}^{(1)} - i \frac{k_x}{k_x^2 + k_y^2} \hat{\Lambda}^{(1)}.$$

It follows from (30) that imposition of the dispersion relation $\omega = k_z$ implies that $\Lambda^{(1)}$ is indeterminate. We can, however, determine the first-order compressibility $\chi^{(1)}$ as follows. Putting $k_x = k_\perp \cos\theta$, $k_y = k_\perp \sin\theta$, we find that (40) becomes

$$\left(\sin 2\theta k_\perp \frac{\partial}{\partial k_\perp} + \cos 2\theta \frac{\partial}{\partial \theta}\right) \hat{A}(k_\perp, \theta) = -\sin 2\theta \hat{A}(k_\perp, \theta), \tag{42}$$

while (41) reduces to

$$\hat{\chi}^{(1)} = \cos 2\theta \frac{1}{k_\perp} \frac{\partial}{\partial k_\perp} (k_\perp^2 \hat{A}) - \sin 2\theta \frac{\partial \hat{A}}{\partial \theta}. \tag{43}$$

Introducing $u = \cos 2\theta$, these equations reduce further to

$$\left(k_\perp \frac{\partial}{\partial k_\perp} - 2u \frac{\partial}{\partial u}\right) \hat{A}(k_\perp, u) = -\hat{A}(k_\perp, u), \tag{44}$$

$$\hat{\chi}^{(1)}(k_\perp, u) = i\omega \left[u \frac{1}{k_\perp} \frac{\partial}{\partial k_\perp} (k_\perp^2 \hat{A}) + 2(1 - u^2) \frac{\partial \hat{A}}{\partial u}\right]. \tag{45}$$

The general solution of (44), which can be readily determined via the method of characteristics, can be written in the form

$$\hat{A}(k_\perp, u) = \frac{1}{k_\perp} H(k_\perp^2 u) = \frac{1}{k_\perp} H(k_\perp^2 \cos 2\theta), \tag{46}$$

where H is an arbitrary function. Thus, taking the inverse Fourier transform and setting $x = r\cos\varphi$, $y = r\sin\varphi$, we deduce that the general solution for the zeroth-order stream function is

$$A(r, \varphi) = \frac{1}{2\pi} \int_0^\infty \int_0^{2\pi} H(k_\perp^2 \cos 2\theta) \exp[ik_\perp r \cos(\theta - \varphi)] \, dk_\perp \, d\theta. \tag{47}$$

https://doi.org/10.1017/S0022377808007356 Published online by Cambridge University Press

It should be noted that any choice of H that yields finite values for the perturbed field and velocity components in at least part of the domain is physically acceptable. For the case $H = 1$ (47) gives

$$A(r,\phi) = \int_0^\infty dk_\perp\, J_0(k_\perp r) = \frac{1}{r}, \tag{48}$$

where J_0 is the Bessel function of the first kind of order zero. It is straightforward to verify that this solution satisfies (31). The zeroth-order flow is then given by (28) and (29):

$$\tilde{V}_x^{(0)} = -\frac{\sin\varphi}{r^2}\exp[ik_z(z-t)], \quad \tilde{V}_y^{(0)} = \frac{\cos\varphi}{r^2}\exp[ik_z(z-t)]. \tag{49}$$

The zeroth-order streamlines are thus circles centred on the X-line. From (14) and (15) we find that the zeroth-order field perturbations are given by $\tilde{B}_x^{(0)} = -\tilde{V}_x^{(0)}$, $\tilde{B}_y^{(0)} = -\tilde{V}_y^{(0)}$. Both the flow and the field have a singularity at the X-line, arising from the fact that the assumed Fourier spectrum of the stream function does not fall off sufficiently rapidly with perpendicular wave number to prevent the double integral in (47) from diverging in this limit. The zeroth-order current $\mathbf{j}^{(0)} = \nabla \times \mathbf{B}^{(0)}/\mu_0$ is also singular at the X-line, with $j_z^{(0)}$ diverging as $1/r^3$.

For $H = 1$ we find from (45) that

$$\hat{\chi}^{(1)} = \frac{i\omega\cos 2\theta}{k_\perp}, \tag{50}$$

and hence it follows that

$$\begin{aligned}\chi^{(1)} &= \frac{i\omega}{2\pi}\int_0^\infty\int_0^{2\pi} \cos 2\theta \exp[ik_\perp\cos(\theta-\varphi)]\, dk_\perp\, d\theta \\ &= -i\omega\cos 2\varphi \int_0^\infty J_2(k_\perp r)\, dk_\perp \\ &= -\frac{i\omega\cos 2\varphi}{r},\end{aligned} \tag{51}$$

where J_2 is the Bessel function of the first kind of order two. The first-order compressibility thus has the same azimuthal angle dependence as the equilibrium azimuthal magnetic flux ψ_E, given by (3). We note from (36) and (39) that the first-order z-components of the flow and field also have this azimuthal structure:

$$\tilde{V}_z^{(1)} = \tilde{B}_z^{(1)} = -\frac{\cos 2\varphi}{r}. \tag{52}$$

The fact that these quantities are finite indicates that the wave is no longer polarized in the plane perpendicular to the propagation direction: this, together with the fact that the wave is compressible to first order, is to be expected, since the presence of an X-point is known to cause coupling of the shear and fast Alfvén waves (Bulanov et al. 1992).

The singularity at $r = 0$ in the above solution can be avoided by choosing a different function H in (46). For example, we may set

$$H = \begin{cases} \exp[-k_\perp^2\cos 2\theta], & \cos 2\theta > 0, \\ 0, & \cos 2\theta < 0. \end{cases} \tag{53}$$

https://doi.org/10.1017/S0022377808007356 Published online by Cambridge University Press

It is straightforward to show that the imaginary part of the double integral in (47) vanishes, so that

$$A(r,\varphi) = \frac{1}{\pi}\int_0^{\infty}\int_{-\pi/4}^{\pi/4} \exp[-k_\perp^2 \cos 2\theta]\cos[k_\perp r\cos(\theta-\varphi)]\,dk_\perp\,d\theta. \tag{54}$$

We can reduce this expression to a single integral as follows. The integrand is evidently an even function of $k_\perp$ and therefore we can write

$$A(r,\varphi) = \frac{1}{2\pi}\int_{-\infty}^{\infty}\int_{-\pi/4}^{\pi/4} \exp[-k_\perp^2 \cos 2\theta]\cos[k_\perp r\cos(\theta-\varphi)]\,dk_\perp\,d\theta. \tag{55}$$

The $k_\perp$ integration can then be performed analytically, and (55) reduces to

$$A(r,\varphi) = \frac{1}{2\sqrt{\pi}}\int_{-\pi/4}^{\pi/4} \frac{\exp[-(r^2/4)\cos^2(\theta-\varphi)\sec 2\theta]}{\sqrt{\cos 2\theta}}\,d\theta. \tag{56}$$

Putting $r = 0$, we find that this integral converges and has the value

$$A = \frac{\Gamma(5/4)}{\Gamma(3/4)} \simeq 0.74, \tag{57}$$

where Γ is the gamma function. Indeed the integral converges for all values of r and φ, and can be readily computed numerically for $r \neq 0$. It is of interest to plot the contours of A in the (x, y)-plane, since they represent the streamlines of the zeroth-order flow. These contours are plotted in the upper frame of Fig. 1; the lower frame of this figure is a surface plot of A. A striking contrast is immediately apparent between streamlines in the quadrants $\pi/4 < \varphi < 3\pi/4$, $5\pi/4 < \varphi < 7\pi/4$ and those in the other two quadrants. In the former the streamlines are essentially circles centred on the X-line, as in the previous solution, whereas elsewhere the streamlines are convex towards the X-line: A falls off with distance from the X-line much more rapidly along the x-axis than it does along the y-axis. However, the streamlines in the different regions connect smoothly onto each other at the separatrix. Adopting the current-free X-point configuration as a simple model of the divertor region of a tokamak plasma, it is natural for us to identify the quadrant $\pi/4 < \varphi < 3\pi/4$ as the confined plasma region. The fact that A is finite but evanescent in the two adjoining quadrants (i.e. outside the region of confined plasma, in the tokamak divertor picture) can be interpreted as a manifestation of wave tunnelling through the separatrix. It is apparent from Fig. 1 that the strongest flows occur in this region, close to the X-line.

Using (36) we can also compute $\tilde{V}_z^{(1)}$ for this solution. As noted previously, this quantity can be regarded as a measure of the fast wave amplitude since it is identically zero for a shear wave propagating in the z-direction. After some reduction we obtain

$$\tilde{V}_z^{(1)}(r,\varphi) = -\frac{r^2}{8\sqrt{\pi}}\int_{-\pi/4}^{\pi/4} \frac{(\cos 2\varphi + \cos 2\theta)\exp[-(r^2/4)\cos^2(\theta-\varphi)\sec 2\theta]}{\cos^{3/2} 2\theta}\,d\theta. \tag{58}$$

As in the case of (56), the integral in this expression converges for all r, φ: the contours of $\tilde{V}_z^{(1)}$ are plotted in the upper frame of Fig. 2, with solid (broken) curves representing positive (negative) values of this quantity. The lower frame

https://doi.org/10.1017/S0022377808007356 Published online by Cambridge University Press

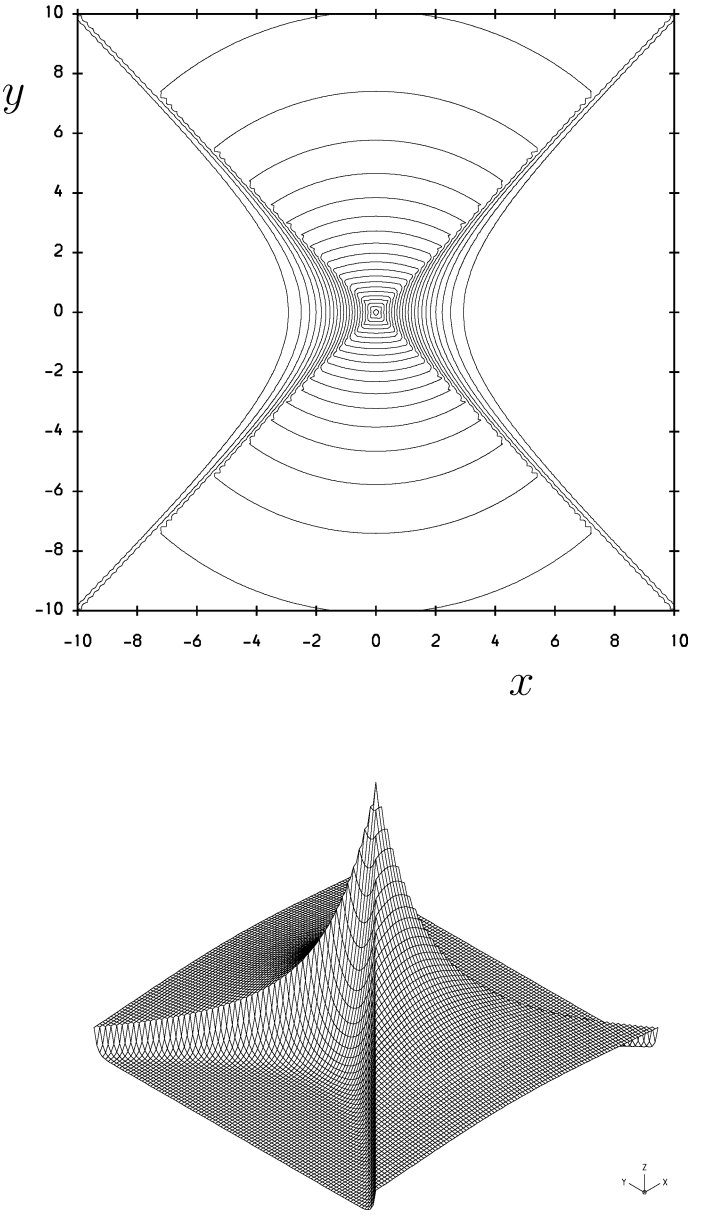


Figure 1. Contour (top) and surface (bottom) plots of $A(x, y)$, i.e. streamlines of the zeroth-order flow, when $H = \exp(-k_\perp^2 \cos 2\theta)$ for $\cos 2\theta > 0$, $H = 0$ for $\cos 2\theta < 0$. The fine-scale structure apparent in the contours close to the separatrix is a computational artefact.

of Fig. 2, which is a surface plot of $\tilde{V}_z^{(1)}$, clearly shows that the absolute value of this quantity is strongly peaked in the vicinity of the separatrix, although it also increases with distance from the X-line and vanishes at this point. Thus, the shear wave is most strongly coupled to the fast wave on the separatrix far from the X-line. Elsewhere, the $\tilde{V}_z^{(1)}$ eigenfunction has a rather complex structure, with O-points in

https://doi.org/10.1017/S0022377808007356 Published online by Cambridge University Press

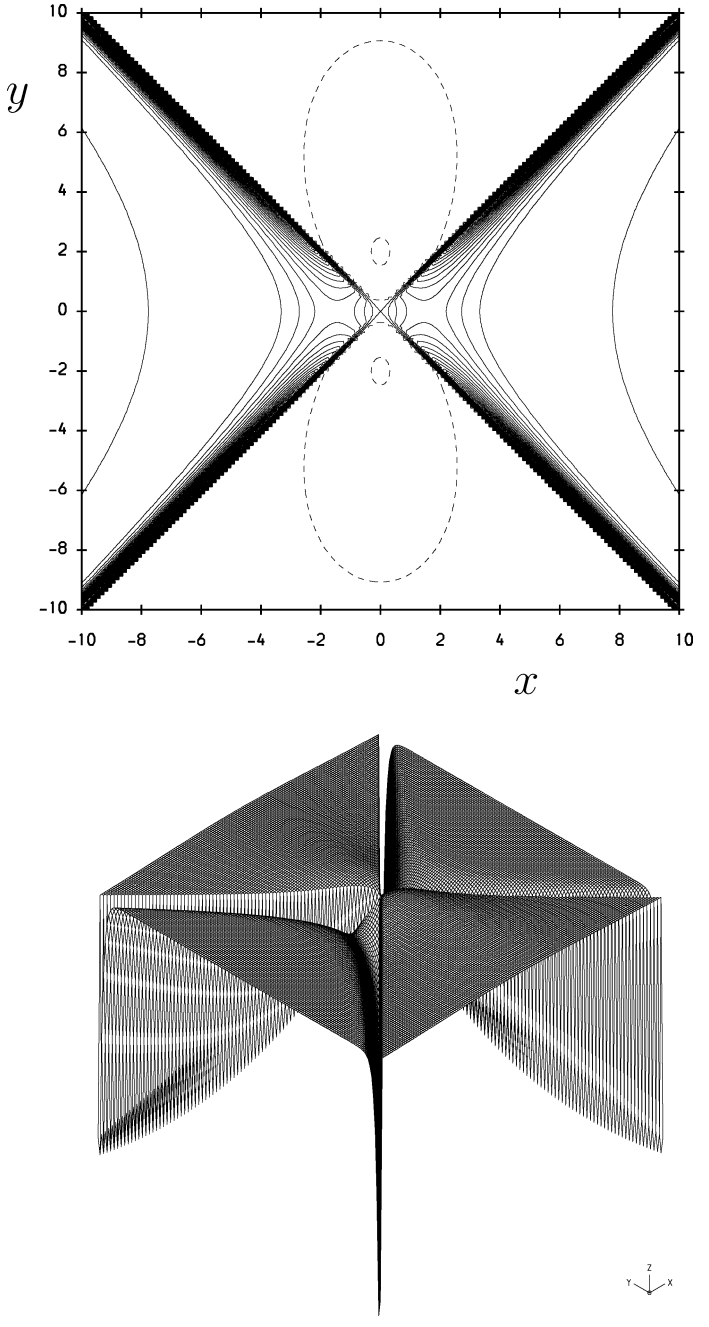


Figure 2. Contour (top) and surface (bottom) plots of $\tilde{V}_z^{(1)}(x, y)$ when $H = \exp(-k_\perp^2 \cos 2\theta)$ for $\cos 2\theta > 0$, $H = 0$ for $\cos 2\theta < 0$. In the contour plot solid and dashed curves indicate respectively $\tilde{V}_z^{(1)} < 0$ and $\tilde{V}_z^{(1)} > 0$. The fine-scale structure apparent in the contours close to the separatrix is again a computational artefact.

https://doi.org/10.1017/S0022377808007356 Published online by Cambridge University Press

the quadrants $\pi/4 < \varphi < 3\pi/4$, $5\pi/4 < \varphi < 7\pi/4$ and secondary X-points in the other two quadrants.

4. Conclusions and discussion

We have presented a linear analysis of Alfvén waves propagating along the X-line of a magnetic X-point configuration with a strong longitudinal field, in the limit of vanishing plasma beta and equilibrium plasma current. This scenario provides a simplified description of Alfvén wave propagation in the divertor region of tokamak plasmas. The presence of the X-point means that the structure of the leading-order (shear Alfvén) eigenfunction is not arbitrary: we have obtained a general solution for the stream function A describing the leading-order flow, and evaluated explicitly both this solution and fast wave corrections to it for two illustrative cases. In the first of these A is azimuthally symmetric in the X-point plane and singular at the X-line, while in the second case A is finite everywhere and largely confined to two quadrants in the X-point plane, one of which can be regarded as representing the confined plasma region in a tokamak. For this second scenario we have shown that strong coupling of the shear and fast waves occurs close to the separatrix far from the X-line. Bulanov et al. (1992) also found that the separatrix plays a key role in the coupling of the two modes.

The singularity at the X-line in the case of the azimuthally symmetric solution for the leading-order flow ($A = 1/r$) is of course unphysical, but it is very likely that it could be removed by extending the model to include non-ideal MHD effects, such as the Hall term in the induction equation, (6). It is worth noting that the characteristic length scale below which the Hall term becomes important, namely the ion skin depth c/ω_{pi} (c being the speed of light and ω_{pi} the ion plasma frequency), is typically a few centimetres for tokamak plasmas, and is thus not negligibly small compared to the macroscopic length scale of the system ($\sim$1 m). With this caveat, and the further caveat that the neglect of equilibrium current is less well-justified in the interior of a tokamak plasma than it is at the edge, the $A = 1/r$ solution could have applications to the X-points of magnetic islands. It may be significant in this context that high-frequency ($\sim$400–500 kHz) density fluctuations, possibly indicative of fast wave activity, have been detected using pulsed radar reflectometry close to the X-points of islands in the TEXTOR tokamak (Donné et al. 2005). The solution with non-azimuthally symmetric A, on the other hand, is more likely to have applications to divertor X-points.

Acknowledgements

This work was supported by the Engineering and Physical Sciences Research Council and by the European Communities under the Contract of Association between EURATOM and UKAEA. The views and opinions expressed herein do not necessarily reflect those of the European Commission.

References

Bulanov, S. V. and Syrovatskii, S. I. 1980 *Sov. J. Plasma Phys.* **6**, 661.

Bulanov, S. V., Shasharina, S. G. and Pegoraro, F. 1992 *Plasma Phys. Control. Fusion* **34**, 33.

Craig, I. J. D. and Watson, P. G. 1992 *Astrophys. J.* **393**, 385.

https://doi.org/10.1017/S0022377808007356 Published online by Cambridge University Press

Donné, A. H., van Gorkom, J. C., Udintsev, V. S., Domier, C. W., Krämer-Flecken, A., Luhmann Jr., N. C., Schüller, F. C. and TEXTOR team 2005 *Phys. Rev. Lett.* **94**, 085001.

Farina, D., Pozzoli, R. and Ryutov, D. D. 1993 *Nucl. Fusion* **33**, 1315.

Kirk, A. et al. 2006 *Plasma Phys. Control. Fusion* **48**, B433.

McClements, K. G., Thyagaraja, A., Ben Ayed, N. and Fletcher, L. 2004 *Astrophys. J.* **609**, 423.

McClements, K. G., Shah, N. and Thyagaraja, A. 2006 *J. Plasma Phys.* **72**, 571.

McClymont, A. N. and Craig, I. J. D. 1996 *Astrophys. J.* **466**, 487.

McKay, R. J., McClements, K. G. and Fletcher, L. 2007 *Astrophys. J.* **658**, 631.

Myra, J. R., D'Ippolito, D. A., Xu, X. Q. and Cohen, R. H. 2000 *Contrib. Plasma Phys.* **40**, 352.

McLaughlin, J. A. and Hood, A.W. 2004 *Astron. Astrophys.* **420**, 1129.

https://doi.org/10.1017/S0022377808007356 Published online by Cambridge University Press